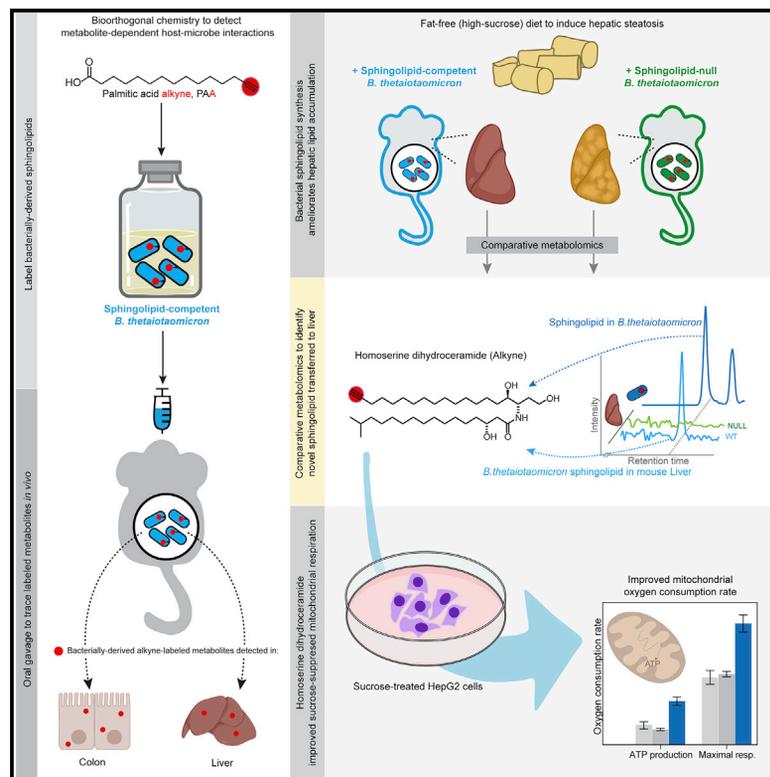# Cell Host & Microbe

Host hepatic metabolism is modulated by gut microbiota-derived sphingolipids

Graphical abstract

Authors

Henry H. Le, Min-Ting Lee,
Kevin R. Besler, Elizabeth L. Johnson

Correspondence

elj54@cornell.edu

In brief

Identifying microbial metabolites modulating metabolism can be challenging. Le et al. use bioorthogonal chemistry to identify and trace the transfer of a unique bacterial sphingolipid to colon and liver tissue. Furthermore, bacterial sphingolipid synthesis by *Bacteroides* was determined to ameliorate hepatic lipid accumulation in a mouse model of hepatic steatosis.

Highlights

- Alkyne-modified lipids used to trace microbe-host metabolite transfer

- Unique bacterial sphingolipid is transferred from the gut microbiome to the liver

- Microbial sphingolipid improves respiration in liver cells

- Bacterial sphingolipid synthesis decreases excess hepatic lipid accumulation

CellPress

Article

Host hepatic metabolism is modulated by gut microbiota-derived sphingolipids

Henry H. Le,[1,2] Min-Ting Lee,[1,2] Kevin R. Besler,[1] and Elizabeth L. Johnson[1,3,*]
[1]Division of Nutritional Sciences, Cornell University, Ithaca, NY 14853, USA
[2]These authors contributed equally
[3]Lead contact
*Correspondence: elj54@cornell.edu
https://doi.org/10.1016/j.chom.2022.05.002

SUMMARY

Microbially-derived gut metabolites are important contributors to host phenotypes, many of which may link microbiome composition to metabolic disease. However, relatively few metabolites with known bioactivity have been traced from specific microbes to host tissues. Here, we use a labeling strategy to characterize and trace bacterial sphingolipids from the gut symbiont *Bacteroides thetaiotaomicron* to mouse colons and livers. We find that bacterial sphingolipid synthesis rescues excess lipid accumulation in a mouse model of hepatic steatosis and observe the transit of a previously uncharacterized bacterial sphingolipid to the liver. The addition of this sphingolipid to hepatocytes improves respiration in response to fatty-acid overload, suggesting that sphingolipid transfer to the liver could potentially contribute to microbiota-mediated liver function. This work establishes a role for bacterial sphingolipids in modulating hepatic phenotypes and defines a workflow that permits the characterization of other microbial metabolites with undefined functions in host health.

INTRODUCTION

Metabolites produced by the gut microbiome are known to modulate trans-kingdom interactions that contribute to host health (Krautkramer et al., 2021). These metabolites have great potential for systemic effects on host pathways, but the identification and functional characterization of many of these metabolites remain elusive. To date, a handful of microbiome-derived metabolites have been found to transit to host tissues, many of which lack defined bioactivity (Donia and Fischbach, 2015). Additionally, although microbiome-derived small molecules have been shown to influence hepatic function (Schroeder and Bäckhed, 2016), further exploration is required to provide evidence demonstrating their direct transfer from the microbiome to the liver. The discovery of microbiome-derived metabolites that transfer to the liver offers therapeutic targets for metabolic disorders stemming from both the molecule of action and the contextual abundance of the microbe of origin.

As microbiome-derived metabolites are diverse, one approach to identifying promising bioactive candidates is to identify metabolites that are produced in both prominent microbes and in their hosts and then determine whether these metabolites are transferred from microbe to host. One such class of metabolites is bioactive sphingolipids (SLs), a class of lipids with well-defined roles in mammalian energy metabolism pathways (Summers et al., 2019) that are readily synthesized by prominent gut microbes of the genera *Bacteroides* (Kato et al., 1995; Stoffel et al., 1975) and *Prevotella* (LaBach and White, 1969). Microbial SL production has been characterized in a variety of successful systems of host-

microbe symbioses, ranging from choanoflagellates to plants to mammals (Heaver et al., 2018). As mammalian sphingolipids play important roles in host biology, it is possible that microbiome-derived SLs also influence host phenotypes through pathways ranging from proliferation to insulin signaling (Hannun and Obeid, 2018). Known roles for bacterial SLs in immune system modulation include the modulation of natural killer T cells via glycosphingolipids produced by *Bacteroides fragilis* (An et al., 2014) and decreased intestinal inflammation in *Bacteroides thetaiotaomicron* monoassociated mice (Brown et al., 2019). Despite the promising candidate effects of bacterial SLs on host physiology, mammalian host-microbe SL-specific bioactivities are mostly limited to aspects of the colon and perturbations in local immunity. Although it is known that bacterial SL production can alter SL levels in the liver (Johnson et al., 2020), the physiological effects of SL synthesis on host hepatic phenotypes and whether intact SLs transfer from the microbiome to the liver to affect host metabolism are unknown. Based on the knowledge that palmitic acid-derived lipids from *B. thetaiotaomicron* can enter host tissue (Johnson et al., 2020), we endeavored to identify these lipids, determine whether they transit to the liver, and determine whether they may modulate hepatic metabolic phenotypes.

RESULTS

Bioorthogonal labeling of lipids to monitor sphingolipid synthesis in *Bacteroides thetaiotaomicron*

To investigate bacterially-derived SL transfer to mammalian hosts, we developed a method to trace SL transfer *in vivo* that

leverages bioorthogonal chemistry by labeling newly synthesized bacterial SLs with palmitic acid alkyne (PAA; a proxy for palmitic acid) in culture, orally introducing these cultures into mice, and monitoring the transfer of alkyne-modified lipids using fluorescence detection and comparative metabolomics (Figures 1A and 1B). To support this approach, we created a catalog of the PAA-derived sphingometabolome of *B. thetaiotaomicron* to determine if any of these *Bacteroides*-derived lipids were transferred to mammalian hosts. The SLs that we cataloged are the set detectable using our approach and do not represent the full diversity of *B. thetaiotaomicron* SLs. Included in our analysis are SLs produced through *de novo* synthesis. More specifically, *de novo* SL biosynthesis begins with the condensation of an amino acid and a fatty-acyl CoA via the enzyme serine palmitoyltransferase (SPT) to form a 3-ketosphingoid base. These 3-ketosphingoid bases are converted to sphingoid bases (SBs), which can then be tailored to form more complex SLs (Figure 1C). Although a diverse array of fatty-acyl CoAs have been described in the first step of SL biosynthesis, the most recognized is palmitic acid.

As previously described (Lee et al., 2021), fluorescence-based detection of alkyne molecules via chemical ligation (click chemistry) to Alexa Fluor-647 azide (AF647-Az) confirmed the uptake of PAA into wild-type *B. thetaiotaomicron* (BTWT) (Figure 1B). A biosynthetic mutant of *B. thetaiotaomicron* that lacks SPT activity (SLMUT) is known to have a similar level of PAA uptake to that of BTWT, but the PAA-derived lipids in SLMUT had not been identified. To identify PAA-derived metabolites, we cultured BTWT and SLMUT with and without PAA and extracted their corresponding metabolomes, which were then subjected to reverse-phase liquid chromatography coupled to high-resolution mass spectrometry (LC-MS) (Figure 1B). Analysis via untargeted comparative metabolomics revealed differential metabolic features representing chemical formulas associated with alkyne-bearing lipids (Figure 1D; Tables S1A and S1B). To further elucidate candidate alkyne-bearing lipids, differential features were subjected to tandem mass spectrometry. Careful analysis of high-resolution MS2 spectra revealed alkyne-bearing SBs (Figure S1), dihydroceramides (DHCers) (Figure S2), dihydroceramide phosphoethanolamides (DHCer-PEs) (Figure S3), dihydroceramide phosphoinositols (DHCer-PIs) (Figure S4), and various glycerolipids (monoacylglycerides and diacylglycerides) (Figure S5). Consistent with these elucidations, we found the complete abolishment of SLs and exaggeration of glycerolipids in SLMUT (Figure 1D). Because SLMUT is a *B. thetaiotaomicron* mutant devoid of PAA-labeled SLs, we used it to determine the SL-specific contributions of the microbiome to hepatic lipid metabolism.

A *B.-thetaiotaomicron*-derived sphingolipid is transferred from the microbiome to the colon and liver

We next sought to determine whether unique bacterial lipids were transferred from the microbiome to host tissues with metabolic functions. To ensure that the lipids being traced were definitively derived from *B. thetaiotaomicron*, we used our lipid tagging system in BTWT and SLMUT with PAA (Figure 2A). Bioorthogonal labeling of lipids in *B. thetaiotaomicron* permits the visualization of *B.-thetaiotaomicron*-derived lipids that transit to host systems. Alkyne-containing lipids from *B. thetaiotaomicron* were visualized in host tissues through the chemical ligation of the fluorophore AF647-Az (red) using click chemistry. BTWT and SLMUT cultures were grown in the presence of PAA before being orally introduced to mice (BTWT[PAA] and SLMUT[PAA]) (Figure 2B). Lipids were excluded from the diet to ensure the detection of host-assimilated bacterially-derived lipids. Specific pathogen-free mice were placed on this fat-free (high-sucrose) diet for one month before the daily oral introduction of BTWT[PAA] or SLMUT[PAA] cultures for 1 week (Figure 2B). After 1 week, mice were sacrificed and tissues were collected. Similar levels of alkyne-tagged lipids were observed in the cecal contents of both BTWT[PAA]- and SLMUT[PAA]-treated mice (Figure 2C). Surprisingly, alkyne-tagged lipids were detected at a much higher abundance in the tissues of BTWT[PAA] mice as compared with SLMUT[PAA] mice (Figure 2C), suggesting that bacterial SL synthesis enhances metabolite transfer to host tissues. Click-chemistry-based detection showed that BTWT[PAA]-derived metabolites were transferred to the colonic and hepatic tissue of BTWT[PAA] mice (Figure 2C). Transfer was not observed when bacterial cultures were heat killed (Figure S6F), suggesting that an active process may be necessary for the observed effects of bacterial SL transfer on host tissue.

To determine whether the transferred metabolites were SLs, we searched for alkyne-containing versions of the *Bacteroides* SLs characterized in colon and liver tissue (Figure 1D). Targeted analyses revealed no detectable levels of serine-, alanine-, or threonine-derived bacterial SLs (Figures 2D and S7). Intriguingly, an unidentified mass that might be a bacterially derived dihydroceramide was detected in the colon and liver of BTWT[PAA] mice and was absent from all control mice (Figures 2D and S8). This uncharacterized mass at the identical retention time was also detected in our profiling of the bacterial sphingolipidome, making it a candidate bacterial SL that is transferred from the microbiome to host tissue. Despite extensive efforts to characterize other *B.-thetaiotaomicron*-derived lipids that transit to the liver, thus far, our methods have detected only this specific candidate SL. It is possible and likely that other derivatives of bacterially-produced SLs transfer to host tissue but were not captured by our detection methods.

B. thetaiotaomicron synthesizes a set of homoserine-containing sphingolipids that are transferred to host tissues

To identify the uncharacterized SL transferred from *B. thetaiotaomicron* to the liver, we embarked on a deeper analysis of the sphingolipidome from Figure 1D. Comprehensive analysis of MS2 spectra of serine-derived SLs revealed a strong fragment at *m/z* 60.04 (Figures S1 and S2). Interestingly, two differential PAA-dependent DHCers with chemical formulas of $C_{36}H_{69}NO_4$ had fragmentation patterns inconsistent with those of the serine-derived SLs and instead showed a pronounced fragment at *m/z* 74.06 (Figures S1 and S2). To determine the identity of these unique SLs, we incubated BTWT cultures with stable amino acid isotopes. Feeding of isotopically enriched L-serine to BTWT resulted in efficient labeling of serine-based SLs; however, serine failed to label the unknown DHCer (Figures 3A, 3B, and S9). Although L-serine is the most recognized amino acid used to construct most known SLs, L-alanine, L-glycine, and L-cysteine can also be used (Duan and Merrill,
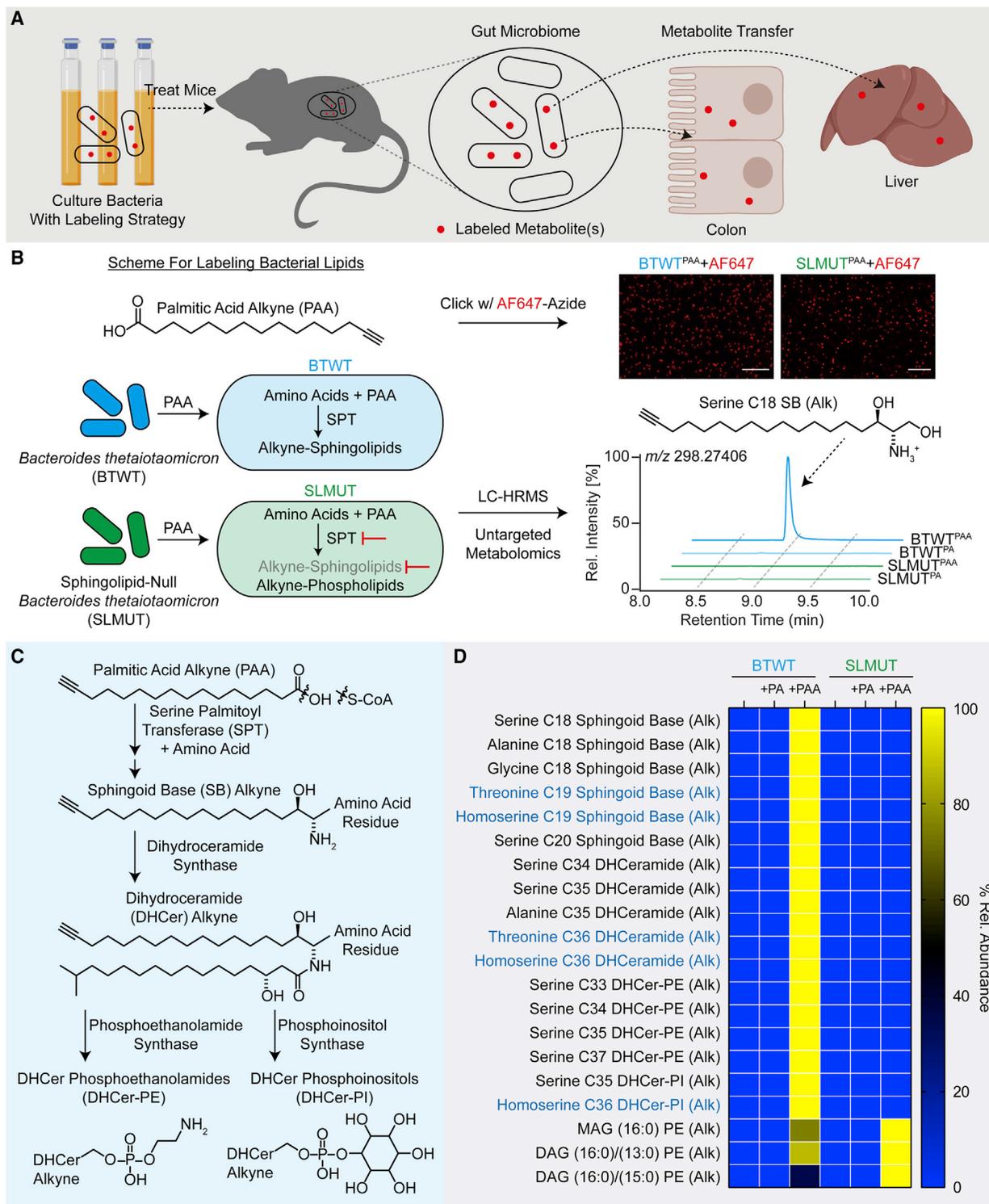
Figure 1. Bioorthogonal labeling of newly synthesized lipids in *B. thetaiotaomicron* allows for detailed mapping of the *Bacteroides* lipidome

(A) Schematic of the strategy to trace bacterial sphingolipid (SL) transfer to host tissue.

(B) Schematic of SL biosynthesis and integration of palmitic acid alkyne (PAA). PAA treatment of either wild-type *B. thetaiotaomicron* (BTWT) or its SL-null mutant (SLMUT), followed by chemical ligation of Alexa Fluor-647 azide and confocal fluorescence microscopy (scale bars, 20 µm) or untargeted differential metabolomic analysis following high-resolution mass spectrometry.

(C) Biosynthetic pathway of SLs synthesized using PAA.

(D) Heatmap of alkyne-bearing SLs following treatment with palmitic acid (PA), PAA, or no treatment. Previously uncharacterized SLs are noted in blue.
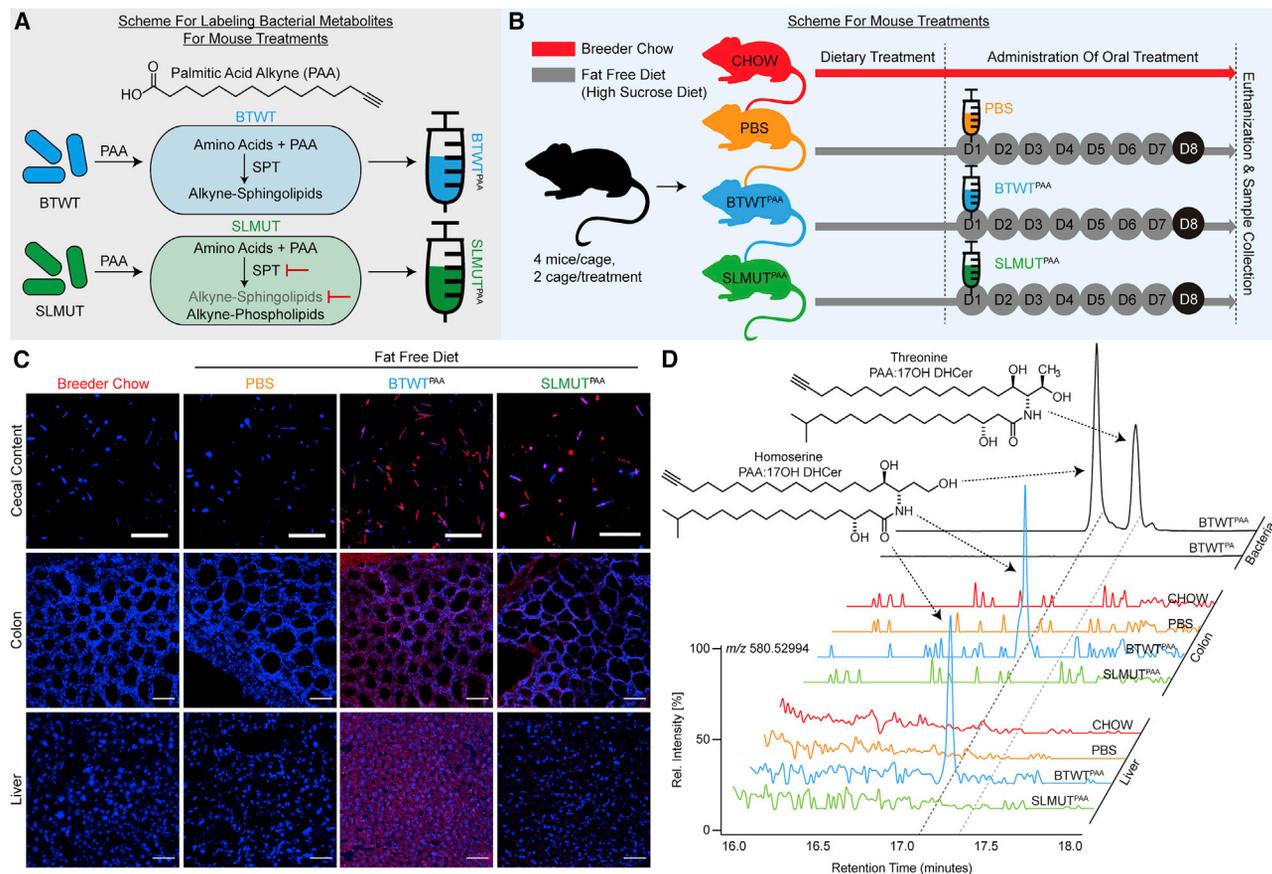
See also Figures S1–S5

Figure 2. BTWT sphingolipids transfer to the colon and liver

(A) Scheme for labeling *B. thetaiotamicron* metabolites with palmitic acid alkyne (PAA) to create BTWT[PAA] and SLMUT[PAA] treatment cultures.

(B) Scheme for treatment of mice fed with either chow or a fat-free diet. Fat-free diet mice were gavaged with either PBS, BTWT[PAA], or SLMUT[PAA].

(C) Confocal images of cecal contents (scale bars, 20 μm), colon (scale bars, 50 μm), and liver (scale bars, 50 μm) tissue. Alkyne-bearing metabolites originating from *B. thetaiotaomicron* are visualized through chemical ligation to Alexa Fluor-647 azide (red). Hoechst 33342 (blue) was used as a DNA stain.

(D) High-resolution mass spectrometry ion chromatograms demonstrating metabolic transfer of homoserine-derived sphingolipids to both colon and liver tissues for BTWT[PAA] samples, which are absent in CHOW, PBS, and SLMUT[PAA] samples.

See also Figures S7 and S8.

2015). The chemical formulas of the unidentified DHCer suggested that the SPT-dependent metabolites did not originate from alanine, glycine, or cysteine. Additionally, feeding of isotopically labeled L-alanine, L-glycine, and L-cysteine failed to label the unidentified DHCer (Figure S9). Further analysis of the chemical formula suggested that the cognate amino acid(s) were effectively serine plus an additional methylene (+CH_2). Three candidate amino acids share this chemical formula: threonine, allothreonine, and homoserine. C13-isotopically enriched L-threonine successfully labeled the unidentified DHCer at a retention time (rt) of 17.4 min, verifying the biosynthetic use of threonine as a previously uncharacterized modular component of sphingolipids (Figures 3A, 3B, and S9B).

Intriguingly, the unidentified DHCer at rt = 17.1 min was not labeled with L-threonine, suggesting that its cognate amino acid was either allothreonine or homoserine (Figure S9C). As neither allothreonine nor homoserine was available commercially in isotopically enriched form, we sought to determine their integration via enzymatic methods. To initiate this, we recombinantly

expressed and purified *B. thetaiotaomicron* SPT (*Bt*SPT) (Figure S10). Fatty-acyl CoAs were then conjugated to specific amino acids with recombinant *Bt*SPT, giving rise to their respective ketosphingoid SL precursors (Figure 3C). The precursors were then fed to SLMUT, which has no native SPT activity; therefore, SL biosynthesis can continue only with the supplied precursor. We found that SLMUT supplied with the L-homoserine-derived ketosphingoid base successfully produced the unknown DHCer at rt = 17.1 min (Figures 3B and 3C). MS2 fragmentation patterns of native L-homoserine-derived DHCers were identical to those produced through amino acid-selective SL biosynthesis (Figures S11A and S11B). As L-homoserine can be derived from either L-methionine or L-aspartic acid, we carried out C13-isotopic studies using these amino acids. Although L-methionine failed to label any SLs, L-aspartic acid successfully labeled the L-homoserine SL, strongly suggesting that L-homoserine-derived SLs are constructed using the homoserine/threonine biosynthetic pathway (Figures 3A–3C). As anticipated, fragmentation analysis of the L-homoserine SL from the
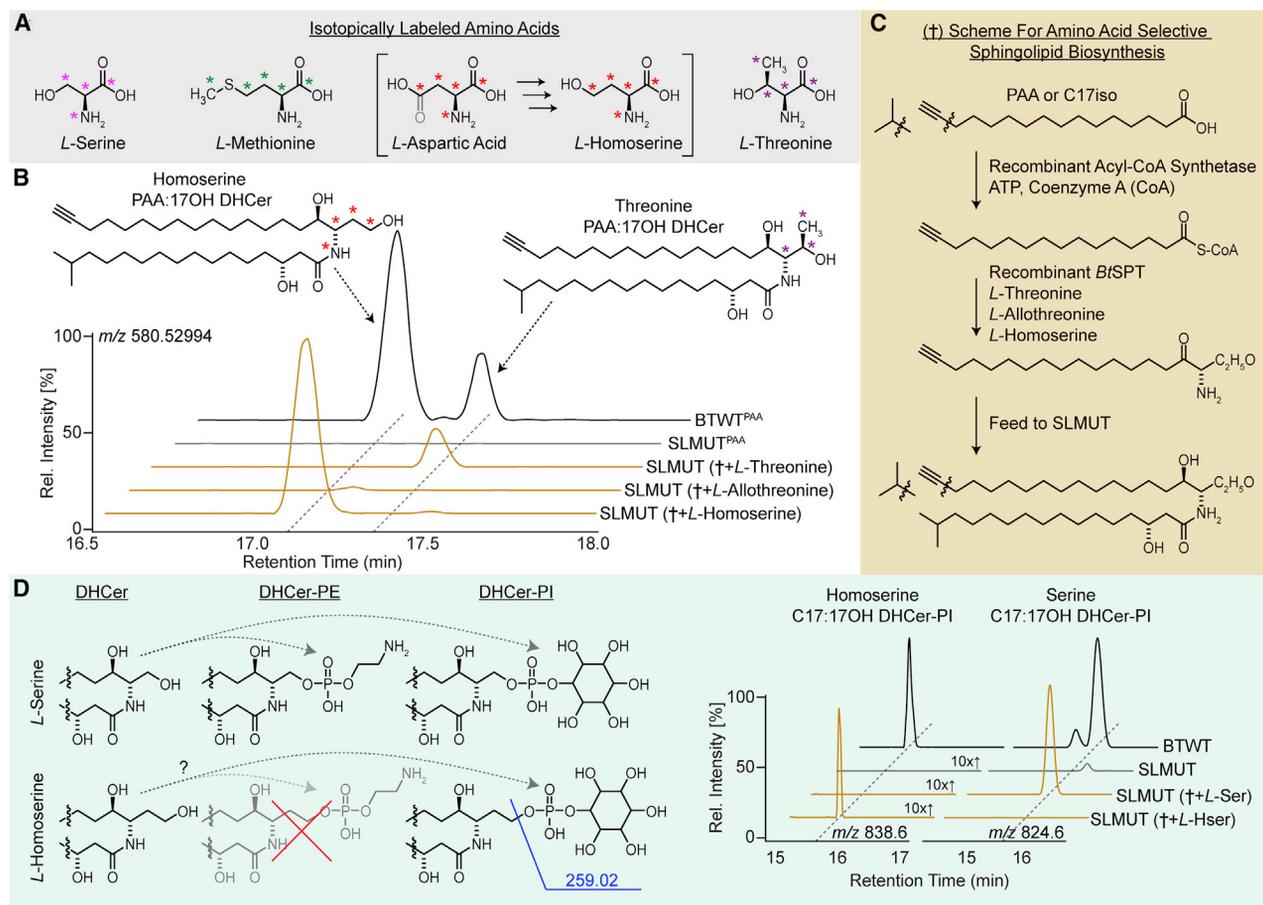
Figure 3. Identification of homoserine- and threonine-derived sphingolipids

(A) Isotopically labeled amino acids used in this study with asterisks (*) marking labeled atoms.

(B) Ion chromatograms and representative structures of homoserine- and threonine-derived dihydroceramides (DHCers) detected in BTWT as well as SLMUT via amino acid-selective biosynthesis. Red and purple asterisks (*) mark isotopic labels observed via heavy L-aspartic acid and L-threonine feeding, respectively.

(C) Scheme for amino acid-selective sphingolipid biosynthesis.

(D) Amino acid-selective sphingolipid biosynthesis demonstrates that homoserine-based DHCers are converted to DHCer-PI and not to DHCer-PE in vivo.

See also Figures S9–S11

isotopically enriched L-aspartic acid treatment identified labeled atoms in the amino acid portion of the SL, ruling out stochastic labeling (Figures S11C–S11E). In vitro analysis of BtSPT activity on 1 mM individual amino acids operating on 0.25 mM palmitoyl-CoA for 1 h at 37°C suggested that serine provides the highest product formation activity, with modest activities observed for L-homoserine and L-alanine (Figure S10C); however, further enzymatic analysis will be required to determine comprehensive substrate parameters. Finally, amino acid-selective SL biosynthesis showed that the fates of homoserine-derived SLs diverge from those constructed from serine, as DHCer-PEs and DHCer-PIs were constructed from serine; however, only DHCer-PIs were observed in homoserine-derived SLs (Figures 3D and S4).

Homoserine sphingolipids alter oxidative respiration and fat accumulation in liver cells

To reveal biology associated with bacterially derived homoserine-DHCers, we endeavored to isolate this SL from

B. thetaiotaomicron to test its activity on liver cells (HepG2 cell line). With methods similar to those mentioned above, we used a coupled in vitro and in vivo scheme to direct B. thetaiotaomicron to only synthesize homoserine-DHCer (STAR Methods). By using purified BtSPT to produce the homoserine-containing long-chain base (Figure 3C), we then added this precursor to a culture of a B. thetaiotaomicron strain harboring mutations lacking SPT and inositol synthesis, effectively forcing B. thetaiotaomicron to produce the SL we observed in the liver. Lipids from this culture were then extracted and fractionated via silica and reverse-phase chromatography. Fractions at each stage containing the homoserine-DHCer were pooled and dried, effectively yielding highly enriched homoserine-DHCer.

To mimic the metabolic conditions of mice exposed to a high-sucrose fat-free diet, HepG2 cells were pre-cultured with a previously characterized high-sucrose media that ultimately promotes lipid accumulation (Softic et al., 2019). To reveal molecular mechanisms of homoserine-DHCer on hepatocytic metabolism, we performed RNA-seq analysis on HepG2 cells treated with
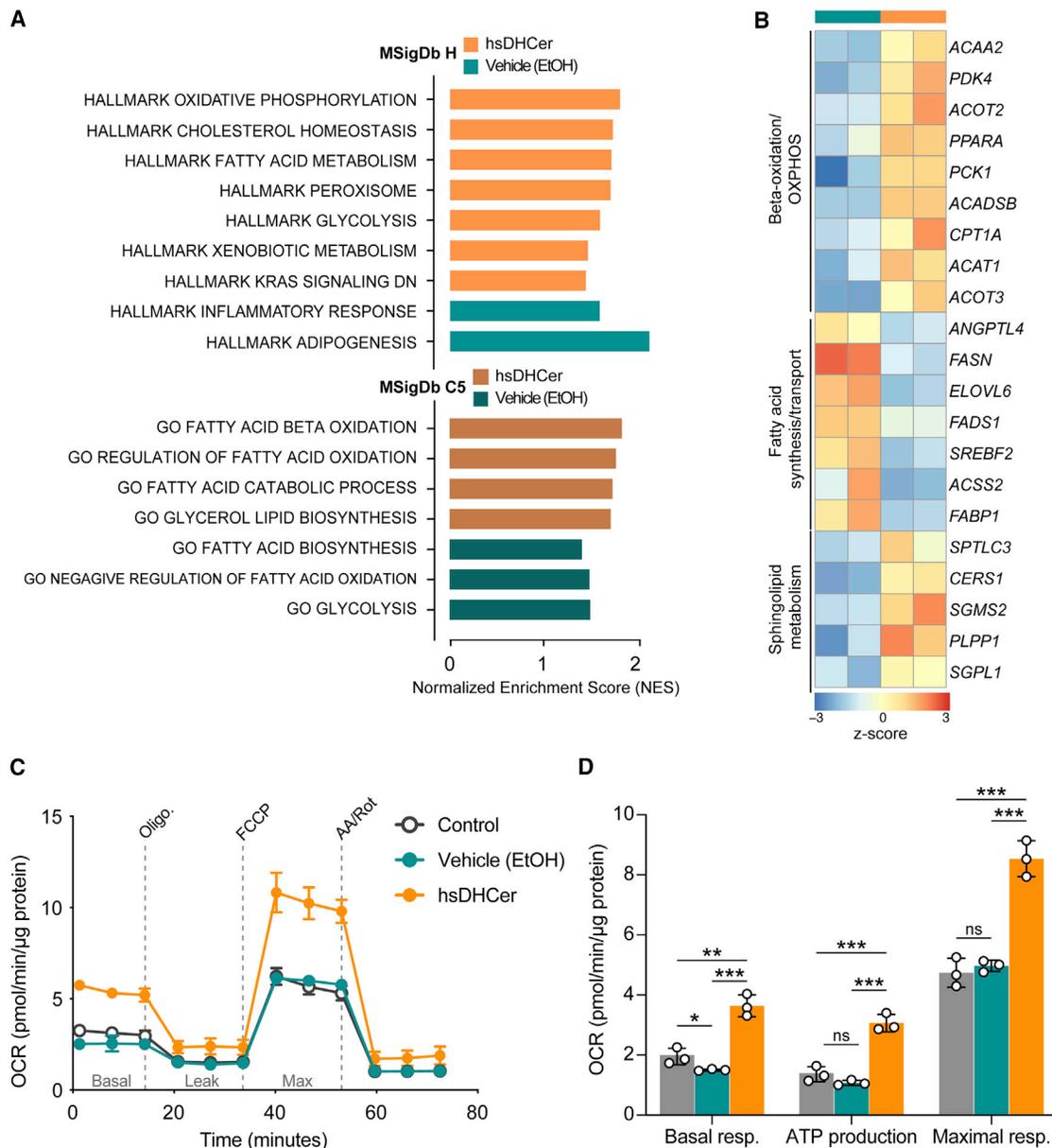
Figure 4. Treatment of liver cells with homoserine dihydroceramide improves cellular respiration

(A) Enriched gene sets in homoserine-DHCer (hsDHCer)-treated HepG2 cells as compared with vehicle-treated controls (n = 2).

(B) Expression heatmap of significantly upregulated or downregulated genes in HepG2 cells treated as described in (A).

(C) Oxygen consumption rate (OCR) of sucrose-conditioned HepG2 cells treated with hsDHCer, ethanol as a vehicle control (vehicle, EtOH) or untreated (control) (n = 3).

(D) Estimation of basal respiration, ATP production, and maximal respiration in the same conditions as (C) based on Seahorse measurement of cellular OCR (n = 3). Data are presented as mean ± SD, one-way ANOVA, p > 0.05: ns, *p ≤ 0.05, **p ≤ 0.01, and ***p ≤ 0.001.

homoserine-DHCer. Gene set enrichment analysis (GSEA) of differentially expressed genes in HepG2 cells treated with homoserine-DHCer compared with cells treated with a vehicle control showed enrichment of pathways engaged in oxidative phosphorylation, fatty-acid metabolism, and glycolysis (Figure 4A; Tables S1C and S1D). These results suggest the reversal of high sugar/fatty-acid-induced energy dysregulation (Softic et al., 2019; Zhang et al., 2017). Further analysis of our homoserine-DHCer treated system shows upregulation of specific genes

involved in β-oxidation and SL metabolism, and downregulation of genes involved in fatty-acid synthesis and transport (Figure 4B; Table S1C). With these findings, we envisioned that homoserine-DHCer promotes mitochondrial respiration, an activity that is suppressed in sucrose-treated HepG2 cells. To this end, we measured the oxygen consumption rate (OCR) in these liver cells. Consistent with our transcriptomic data, homoserine-DHCer treated liver cells showed increased respiration as compared with cells treated with a vehicle control (Figures 4C
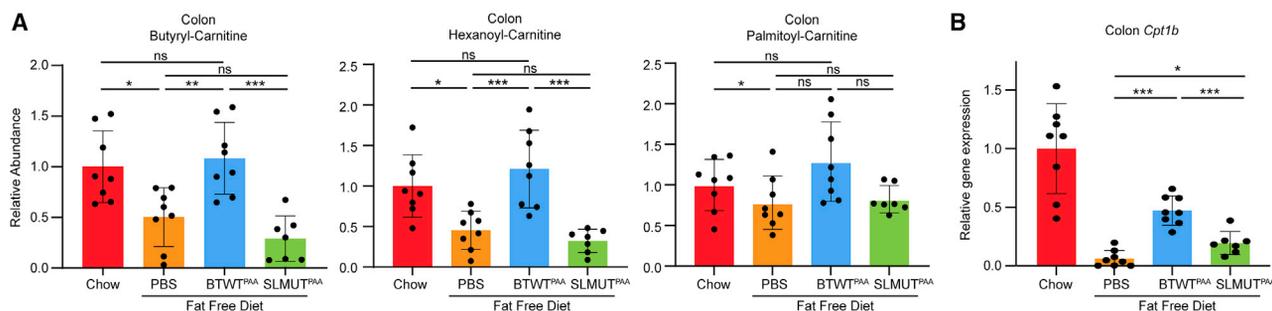
Figure 5. Bacterial sphingolipid production in mice with hepatic steatosis restores colon carnitine levels and expression of *Cpt1* to levels observed in control mice

Mice were fed either chow (Chow) or a fat-free diet. Mice receiving the fat-free diet were gavaged with either PBS, BTWT^{PAA}, or SLMUT^{PAA}.

(A) Relative measurements of butyryl-, hexanoyl-, and palmitoyl-carnitines from treated samples (n = 8).

(B) Relative gene expression measured via RT-qPCR of *Cpt1* in mice colon tissue following treatment (n = 8). Values were normalized to Chow = 1. All values are mean ± SD, one-way ANOVA, $p > 0.05$: ns, $*p \le 0.05$, $**p \le 0.01$, and $***p \le 0.001$.

and 4D; Table S1E). Taken together, these results suggest that homoserine-DHCer modulates metabolic demands for high-sucrose challenged liver cells.

Fatty-acid metabolism is altered in mice with a microbiome active in sphingolipid synthesis

Homoserine-DHCer-dependent respiration changes noted in cultured liver cells prompted us to further investigate altered fatty-acid metabolism in our BTWT^{PAA}/SLMUT^{PAA} mouse model. Noting that targeted analysis revealed bacterial SLs in the colon tissue of BTWT^{PAA} mice (Figures 2D and S8), we carried out untargeted metabolomic analysis among our samples to identify any changes in metabolites other than SLs. Comparative analysis revealed that the BTWT^{PAA} mice contained significantly higher levels of acyl carnitine compared with SLMUT^{PAA} and PBS control mice (Figure 5A). Notably, the acyl carnitines were unlabeled, suggesting that they originated, at least in part, as the result of host processes and not necessarily through direct transfer of bacterial metabolites. Because acyl carnitines are generated by carnitine palmitoyltransferase enzymes and homoserine-DHCer treatment of cells upregulates carnitine palmitoyltransferase (*cpt1*) gene expression (Figure 4B), we measured *Cpt1* transcript levels in the colon tissue from our experimental mice. We noted that BTWT^{PAA} *Cpt1* levels were significantly higher in BTWT^{PAA} samples compared with samples from SLMUT^{PAA} and PBS mice, suggesting that increased CPT1 activity is a potential link between acyl carnitine levels and BTWT^{PAA}-specific host modulating biology (Figure 5B). Additionally, acyl carnitine and CPT1 levels in mice fed chow without bacterial intervention were similar to those of mice that received BTWT^{PAA} treatment while on the fat-free diet. Furthermore, increased CPT1 activity and carnitine levels are known markers of increased fatty-acid processing and mitochondrial β-oxidation, indicating a role for bacterial sphingolipids in the modulation of host lipid processing in the colon. These results, together with the capacity of BTWT to transfer bacterially-derived metabolites to colonocytes, suggest a link between the transfer of unique bacterial lipids and host colon lipid metabolism. Finally, as colon biology can affect the entire organism (Robertson, 2007), determining that fatty-acid metabolism is altered in the colon tissue of BTWT^{PAA} mice has implications for influencing the metabolic state of other major organs.

Diet-induced hepatic steatosis is ameliorated by gut microbiome sphingolipid production

To understand the broader metabolic consequences of bacterial SL biosynthesis and transfer from the gut microbiome, we monitored hepatic lipid-dependent metabolic phenotypes. Two weeks on a fat-free diet results in excess hepatic lipid accumulation and the onset of hepatic steatosis (Kovatcheva-Datchary et al., 2019). In our study, mice fed a fat-free diet (0% fat, 75.9% carbohydrate, and 24.1% protein by kcal) for 1 month had significantly greater hepatic lipid accumulation as compared with mice on a chow diet (23.7% fat, 53.2% carbohydrate, and 23.1% protein by kcal), as shown by H&E staining (Figure 6A) and quantification of hepatic triglyceride levels (Figure 6B). Excess lipid accumulation in mice given a fat-free diet was ameliorated when mice were treated with daily gavages of BTWT^{PAA} for 7 days (Figures 6A and 6B). BTWT^{PAA} mice have significantly lower hepatic triglyceride levels than SLMUT^{PAA} mice and hepatic triglyceride levels are indistinguishable from those of mice fed a chow diet (Figure 6B).

We also observed that the expression of genes involved in lipid metabolism was significantly altered with BTWT^{PAA} exposure (Figure 6D). RNA-seq analysis comparing transcriptomes of livers from BTWT^{PAA} versus SLMUT^{PAA} mice (Table S1F) revealed that genes associated with ceramide synthesis (Figure 6E) and mitochondrial β-oxidation (Figure 6F) were expressed at significantly higher levels in the BTWT^{PAA} condition. In line with our observations in hepatocytes treated with BTWT-derived homoserine-DHCer (Figure 4B), *Cpt1* expression was upregulated in the BTWT^{PAA} state (Figure 6D). Genes involved in inflammation (Figure 6G) and glycerosphingolipid metabolism (Figure 6H) were expressed at significantly lower levels in BTWT^{PAA} mice as compared with SLMUT^{PAA} mice, suggesting that our observed phenotypes are consistent with the previously described role of *B. thetaiotaomicron* sphingolipids in the modulation of inflammation (Brown et al., 2019). These observed gene expression changes in combination with observations of altered carnitine levels in the colons of BTWT^{PAA} mice (Figure 5A) determine a role for bacterial sphingolipid synthesis in influencing host pathways in a manner that could also serve as an indirect contributor to the observed hepatic lipid
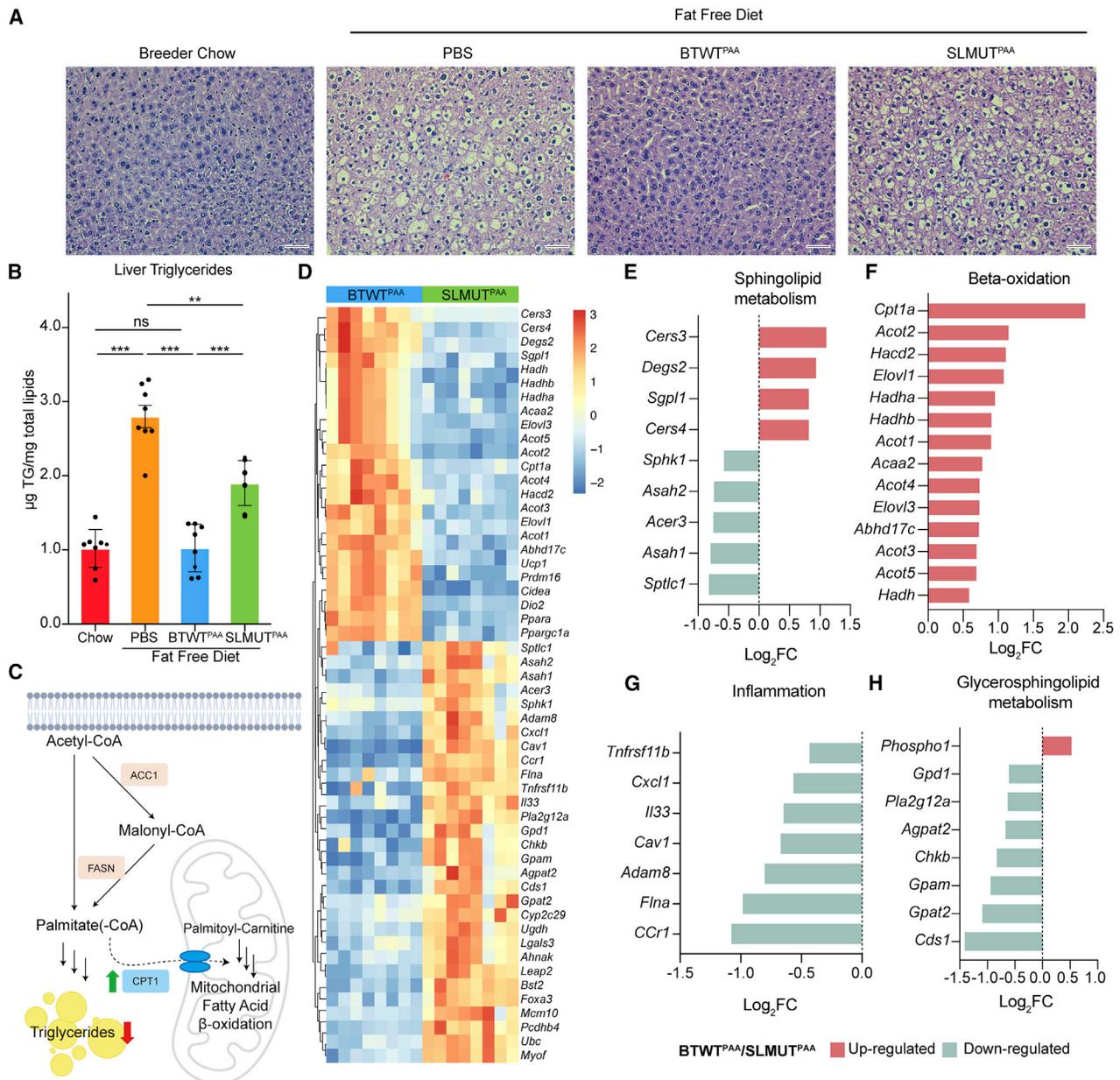
Figure 6. Hepatic steatosis is ameliorated in mice orally gavaged with sphingolipid-competent *B. thetaiotaomicron*

Mice were fed either chow (Chow) or a fat-free diet. Mice receiving the fat-free diet were gavaged with either PBS, BTWT[PAA], or SLMUT[PAA]

(A) Hematoxylin and eosin staining of cross-sectioned liver tissue following the treatments noted above (scale bars, 50 μm).

(B) Total liver triglycerides measured via the triglyceride E test Wako kit (n = 8). Values were normalized to Chow = 1. Values are mean ± SD, one-way ANOVA, p > 0.05: ns, *p ≤ 0.05, **p ≤ 0.01, and ***p ≤ 0.001.

(C) Schematic of various enzymes engaged in fatty-acid metabolism.

(D) Heatmap of significantly differentially expressed hepatic genes in BTWT[PAA] compared with SLMUT[PAA] mice (n = 8 per condition). Log$_2$ fold change (FC) of significantly differentially expressed genes belonging to pathways involved in (E) sphingolipid metabolism, (F) β-oxidation, (G) inflammation, and (H) glycerosphingolipid metabolism.

phenotypes. Taken together, our metabolomic and gene expression data from hepatocytes and mouse livers suggest that the transfer of lipids from sphingolipid-producing bacteria may, directly and indirectly, decrease hepatic lipid accumulation induced by a fat-free diet by driving a switch from lipogenesis to β-oxidation.

DISCUSSION

In this study, we used bioorthogonal labeling to tag SLs of *B. thetaiotaomicron* with PAA, ultimately determining that a bacterial SL transfers from the microbiome to the liver. In monitoring the *Bacteroides* sphingolipidome, we observed previously

uncharacterized SLs with sphingoid bases containing threonine and homoserine. We observed the transit of the homoserine-containing bacterial SLs to the colon and livers of mice. For this study, we focused on the palmitic-acid-derived sphingolipidome and it is very possible that expansion of monitored lipids could lead to the identification of additional sphingolipids that transfer to host tissue. This transfer was not observed using a mutant strain of *B. thetaiotaomicron* that is unable to synthesize SLs *de novo*. In culture, these lipids induced the expression of genes involved in β-oxidation and significantly improved respiration in hepatocytes incubated with excess sucrose. Importantly, hepatic steatosis induced by a fat-free diet in mice was alleviated after 1 week of oral gavage with *B. thetaiotaomicron*. The transfer of the homoserine-containing bacterial SL coincided with the alleviation of hepatic steatosis, suggesting that the metabolic effects of homoserine-DHCer may contribute to the effects of bacterial SL synthesis on hepatic function. Thus, this study adds bacterial SLs to the list of characterized metabolites that transfer to host tissue and can influence host metabolic pathways. Although the transfer of homoserine-DHCer from the microbiota has the potential to influence fatty-acid metabolism in the liver, it is of note that bacterial sphingolipid synthesis most likely contributes to multiple mechanisms that modulate hepatic lipid storage. This is evident by the alterations in host carnitine levels and expression of genes involved in sphingolipid biosynthesis, β-oxidation, and inflammation that were observed in response to *B. thetaiotaomicron* sphingolipid synthesis. Moreover, bacterial sphingolipids have the potential to affect host phenotypes through other indirect mechanisms including facilitating the transfer of other metabolites to the host and through host sensing of sphingolipids in bacterial membranes.

Other gut microbiome-derived metabolites that transit to the liver with defined microbial origins include short-chain fatty acids (Cummings et al., 1987; Neis et al., 2019), tryptophan derivatives (Agus et al., 2018), secondary bile acids (Wahlström et al., 2016), and trimethylamine (TMA) (Bennett et al., 2013; Skye et al., 2018). Here, we present another bacterially-derived molecule that can influence the metabolic state of mammalian hosts. We also observed changes in gene expression that accompanied the transfer of bacterial lipids to the liver, suggesting that bacterial SL synthesis could affect host metabolism by both altering host gene expression and contributing substrates to host metabolism—in addition to other potentially uncharacterized mechanisms.

In addition to furthering our understanding of the importance of bacterial SLs to host metabolism, we overcame some challenges in determining bacterial contributions to host metabolism through the use of bioorthogonal labeling of *B. thetaiotaomicron* lipids to establish the origin and fate of bacterially-produced lipids. The use of PAA and the elimination of lipids from the host diet allowed us to focus on *B.-thetaiotaomicron*-specific lipid transfer without confounding by contributions from diet and other microbes. Given that alkyne-modified precursors to microbial metabolites are readily available, the methods we used to trace bacterial SLs into host metabolism could represent a useful workflow for the identification of other microbial metabolites with uncharacterized functions in hepatic metabolism. Further investigation is also warranted to determine the dynamics of bacterial lipid transfer on diets with various macronu-

trient compositions and if additional SLs or metabolites that originate as bacterial SLs are transferred to host tissue and contribute to host phenotypes.

Sphingolipids are metabolites with the potential to connect diet to microbiome composition to bioactive microbiome-derived metabolites. We documented previously that *Bacteroides* spp. assimilate sphingolipids from the diet (Lee et al., 2021). In our current work, we expand our knowledge of how bacteria that interact with dietary sphingolipids can produce unique sphingolipids that influence host regulatory pathways for hepatic energy metabolism. These observations could provide essential knowledge for using diet or drugs to target *Bacteroides* sphingolipid metabolism for therapeutic use. Together, this work on sphingolipid-dependent host-microbe interactions offers details on how *Bacteroides* SLs can influence host phenotypes and provides an approach for investigating metabolite transfer in other systems of host-microbe interactions.

STAR★METHODS

Detailed methods are provided in the online version of this paper and include the following:

- KEY RESOURCES TABLE
- RESOURCE AVAILABILITY
  - Lead contact
  - Materials availability
  - Data and code availability
- EXPERIMENTAL MODEL AND SUBJECT DETAILS
  - Bacterial strains and conditions
  - Laboratory animals
  - HepG2 cell culture
- METHOD DETAILS
  - Preparation of bacteria for mouse gavage
  - Oral gavage of BTWT[PAA] and SLMUT[PAA] to mice
  - Cu(I)-catalyzed azide-alkyne cycloaddition staining
  - Tissue lipid extraction for LC-HRMS analysis
  - Mass spectrometry analysis
  - Untargeted metabolomic analysis
  - Liver histology
  - qPCR
  - Recombinant *Bt*SPT-His6 purification
  - Synthesis of 3-ketosphinganine derivatives
  - Conversion of 3-KS derivatives to complex SLs
  - Enrichment of homoserine dihydroceramide
  - *In vitro* treatment of homoserine dihydroceramide
  - RNA sequencing and analysis
  - Seahorse extracellular flux measurement
- QUANTIFICATION AND STATISTICAL ANALYSIS

AUTHOR CONTRIBUTIONS

DECLARATION OF INTERESTS

REFERENCES

Agus, A., Planchais, J., and Sokol, H. (2018). Gut microbiota regulation of tryptophan metabolism in health and disease. Cell Host Microbe 23, 716–724. https://doi.org/10.1016/j.chom.2018.05.003.

An, D., Oh, S.F., Olszak, T., Neves, J.F., Avci, F.Y., Erturk-Hasdemir, D., Lu, X., Zeissig, S., Blumberg, R.S., and Kasper, D.L. (2014). Sphingolipids from a symbiotic microbe regulate homeostasis of host intestinal natural killer T cells. Cell 156, 123–133. https://doi.org/10.1016/j.cell.2013.11.042.

Bennett, B.J., de Aguiar Vallim, T.Q., Wang, Z., Shih, D.M., Meng, Y., Gregory, J., Allayee, H., Lee, R., Graham, M., Crooke, R., et al. (2013). Trimethylamine-N-oxide, a metabolite associated with atherosclerosis, exhibits complex genetic and dietary regulation. Cell Metab. 17, 49–60. https://doi.org/10.1016/j.cmet.2012.12.011.

Bolger, Anthony M., Lohse, Marc, and Usadel, Bjoern (2014). Trimmomatic: a flexible trimmer for Illumina sequence data. Bioinformatics 30, 2114–2120. https://doi.org/10.1093/bioinformatics/btu170.

Brown, E.M., Ke, X., Hitchcock, D., Jeanfavre, S., Avila-Pacheco, J., Nakata, T., Arthur, T.D., Fornelos, N., Heim, C., Franzosa, E.A., et al. (2019). Bacteroides-derived sphingolipids are critical for maintaining intestinal homeostasis and symbiosis. Cell Host Microbe 25, 668–680.e7. https://doi.org/10.1016/j.chom.2019.04.002.

Cummings, J.H., Pomare, E.W., Branch, W.J., Naylor, C.P., and Macfarlane, G.T. (1987). Short chain fatty acids in human large intestine, portal, hepatic and venous blood. Gut 28, 1221–1227. https://doi.org/10.1136/gut.28.10.1221.

Denise Robertson, M. (2007). Metabolic cross talk between the colon and the periphery: implications for insulin sensitivity. Proc. Nutr. Soc. 66, 351–361. https://doi.org/10.1017/S0029665107005617.

Dobin, A., Davis, C.A., Schlesinger, F., Drenkow, J., Zaleski, C., Jha, S., Batut, P., Chaisson, M., and Gingeras, T.R. (2013). STAR: ultrafast universal RNA-seq aligner. Bioinformatics 29, 15–21. https://doi.org/10.1093/bioinformatics/bts635.

Donia, M.S., and Fischbach, M.A. (2015). Human microbiota. Small molecules from the human microbiota. Science 349, 1254766. https://doi.org/10.1126/science.1254766.

Duan, J., and Merrill, A.H., Jr. (2015). 1-Deoxysphingolipids encountered exogenously and made de novo: dangerous mysteries inside an enigma. J. Biol. Chem. 290, 15380–15389. https://doi.org/10.1074/jbc.R115.658823.

Goodman, A.L., McNulty, N.P., Zhao, Y., Leip, D., Mitra, R.D., Lozupone, C.A., Knight, R., and Gordon, J.I. (2009). Identifying genetic determinants needed to establish a human gut symbiont in its habitat. Cell Host Microbe 6, 279–289. https://doi.org/10.1016/j.chom.2009.08.003.

Hannun, Y.A., and Obeid, L.M. (2018). Sphingolipids and their metabolism in physiology and disease. Nat. Rev. Mol. Cell Biol. 19, 175–191. https://doi.org/10.1038/nrm.2017.107.

Heaver, S.L., Johnson, E.L., and Ley, R.E. (2018). Sphingolipids in host-microbial interactions. Curr. Opin. Microbiol. 43, 92–99. https://doi.org/10.1016/j.mib.2017.12.011.

Helf, M.J., Fox, B.W., Artyukhin, A.B., Zhang, Y.K., and Schroeder, F.C. (2022). Comparative metabolomics with Metaboseek reveals functions of a conserved fat metabolism pathway in C. elegans. Nat. Commun. 13, 782. https://doi.org/10.1038/s41467-022-28391-9.

Johnson, E.L., Heaver, S.L., Waters, J.L., Kim, B.I., Bretin, A., Goodman, A.L., Gewirtz, A.T., Worgall, T.S., and Ley, R.E. (2020). Sphingolipids produced by gut bacteria enter host metabolic pathways impacting ceramide levels. Nat. Commun. 11, 2471. https://doi.org/10.1038/s41467-020-16274-w.

Kato, M., Muto, Y., Tanaka-Bandoh, K., Watanabe, K., and Ueno, K. (1995). Sphingolipid composition in Bacteroides species. Anaerobe 1, 135–139. https://doi.org/10.1006/anae.1995.1009.

Kovatcheva-Datchary, P., Shoaie, S., Lee, S., Wahlström, A., Nookaew, I., Hallen, A., Perkins, R., Nielsen, J., and Bäckhed, F. (2019). Simplified intestinal microbiota to study microbe-diet-host interactions in a mouse model. Cell Rep. 26, 3772–3783.e6. https://doi.org/10.1016/j.celrep.2019.02.090.

Krautkramer, K.A., Fan, J., and Bäckhed, F. (2021). Gut microbial metabolites as multi-kingdom intermediates. Nat. Rev. Microbiol. 19, 77–94. https://doi.org/10.1038/s41579-020-0438-4.

LaBach, J.P., and White, D.C. (1969). Identification of ceramide phosphorylethanolamine and ceramide phosphorylglycerol in the lipids of an anaerobic bacterium. J. Lipid Res. 10, 528–534.

Lee, M.T., Le, H.H., and Johnson, E.L. (2021). Dietary sphinganine is selectively assimilated by members of the mammalian gut microbiome. J. Lipid Res. 62, 100034. https://doi.org/10.1194/jlr.RA120000950.

Love, M.I., Huber, W., and Anders, S. (2014). Moderated estimation of fold change and dispersion for RNA-seq data with DESeq2. Genome Biol. 15, 550. https://doi.org/10.1186/s13059-014-0550-8.

Neis, E.P., van Eijk, H.M., Lenaerts, K., Olde Damink, S.W., Blaak, E.E., Dejong, C.H., and Rensen, S.S. (2019). Distal versus proximal intestinal short-chain fatty acid release in man. Gut 68, 764–765. https://doi.org/10.1136/gutjnl-2018-316161.

Patro, R., Duggal, G., Love, M.I., Irizarry, R.A., and Kingsford, C. (2017). Salmon provides fast and bias-aware quantification of transcript expression. Nat. Methods 14, 417–419. https://doi.org/10.1038/nmeth.4197.

Schindelin, J., Arganda-Carreras, I., Frise, E., Kaynig, V., Longair, M., Pietzsch, T., Preibisch, S., Rueden, C., Saalfeld, S., Schmid, B., et al. (2012). Fiji: an open-source platform for biological-image analysis. Nat. Methods 9, 676–682. https://doi.org/10.1038/nmeth.2019.

Schroeder, B.O., and Bäckhed, F. (2016). Signals from the gut microbiota to distant organs in physiology and disease. Nat. Med. 22, 1079–1089. https://doi.org/10.1038/nm.4185.

Skye, S.M., Zhu, W., Romano, K.A., Guo, C.J., Wang, Z., Jia, X., Kirsop, J., Haag, B., Lang, J.M., DiDonato, J.A., et al. (2018). Microbial transplantation With human gut commensals containing CutC is sufficient to transmit enhanced platelet reactivity and thrombosis potential. Circ. Res. 123, 1164–1176. https://doi.org/10.1161/CIRCRESAHA.118.313142.

Softic, S., Meyer, J.G., Wang, G.X., Gupta, M.K., Batista, T.M., Lauritzen, H.P.M.M., Fujisaka, S., Serra, D., Herrero, L., Willoughby, J., et al. (2019). Dietary sugars alter hepatic fatty acid oxidation via transcriptional and post-translational modifications of mitochondrial proteins. Cell Metab. 30, 735–753.e4. https://doi.org/10.1016/j.cmet.2019.09.003.

Stoffel, W., Dittmar, K., and Wilmes, R. (1975). Sphingolipid metabolism in Bacteroideaceae. Hoppe Seylers Z. physiol. Chem. *356*, 715–725.

Subramanian, A., Tamayo, P., Mootha, V.K., Mukherjee, S., Ebert, B.L., Gillette, M.A., Paulovich, A., Pomeroy, S.L., Golub, T.R., Lander, E.S., and Mesirov, J.P. (2005). Gene set enrichment analysis: a knowledge-based approach for interpreting genome-wide expression profiles. Proc. Natl. Acad. Sci. USA *102*, 15545–15550. https://doi.org/10.1073/pnas.0506580102.

Summers, S.A., Chaurasia, B., and Holland, W.L. (2019). Metabolic Messengers: ceramides. Nat. Metab. *1*, 1051–1058. https://doi.org/10.1038/s42255-019-0134-8.

Wahlström, A., Sayin, S.I., Marschall, H.U., and Bäckhed, F. (2016). Intestinal crosstalk between bile acids and microbiota and its impact on Host Metabolism. Cell Metab. *24*, 41–50. https://doi.org/10.1016/j.cmet.2016.05.005.

Wieland Brown, L.C., Penaranda, C., Kashyap, P.C., Williams, B.B., Clardy, J., Kronenberg, M., Sonnenburg, J.L., Comstock, L.E., Bluestone, J.A., and Fischbach, M.A. (2013). Production of alpha-galactosylceramide by a prominent member of the human gut microbiota. PLoS Biol. *11*, e1001610. https://doi.org/10.1371/journal.pbio.1001610.

Zhang, Y., Takemori, H., Wang, C., Fu, J., Xu, M., Xiong, L., Li, N., and Wen, X. (2017). Role of salt inducible kinase 1 in high glucose-induced lipid accumulation in HepG2 cells and metformin intervention. Life Sci. *173*, 107–115. https://doi.org/10.1016/j.lfs.2017.02.001.

STAR★METHODS

KEY RESOURCES TABLE

REAGENT or RESOURCE	SOURCE	IDENTIFIER
Bacterial and virus strains		
B. thetaiotaomicron VPI-5482 – BTWT	Goodman Lab, Yale University	
B. thetaiotaomicron VPI-5482 – SLMUT	Goodman Lab, Yale University	
B. thetaiotaomicron iSPTΔ1526	Ley Lab, Max Planck Institute for Developmental Biology	
Chemicals, peptides, and recombinant proteins		
Alkynyl palmitic acid	Click Chemistry Tools	Cat# 1165-100
15-Methyl palmitic acid	Cayman Chemical	Cat# 24814
Palmitic acid	MP Biomedicals	Cat# 02100905-CF
L-Serine	Sigma-Aldrich	Cat# S4500
L-Homoserine	Carbosynth	Cat# FH23855
L-Threonine	Sigma-Aldrich	Cat# T8625
L-Allothreonine	Carbosynth	Cat# FA30577
Palmitoyl coenzyme A potassium salt	Chem Impex	Cat# 01894
Coenzyme A hydrate	Chem Impex	Cat# 00644
Bacto Brain Heart Infusion (BHI)	Becton Dickinson (BD)	Cat# 237500
Potassium phosphate monobasic	Sigma-Aldrich	Cat# P9791
Sodium chloride	Sigma-Aldrich	Cat# S9888
Ammonium sulfate	Fisher Scientific	Cat# AC205872500
D-(+)-Glucose	Sigma-Aldrich	Cat# G7021
Sodium hydroxide	Sigma-Aldrich	Cat# 221465
Hemin	Fisher Scientific	Cat# MP021988202
Magnesium chloride	Sigma-Aldrich	Cat# M8266
Iron (II) sulfate heptahydrate	Sigma-Aldrich	Cat# 215422
Vitamin K3 (Menadione)	Cayman Chemical	Cat# 15950
Calcium chloride	Sigma-Aldrich	Cat# C1016
Vitamin B12	Sigma-Aldrich	Cat# V6629
L-Cysteine hydrochloride	Sigma-Aldrich	Cat# C1276
Sodium thioglycolate	Sigma-Aldrich	Cat# T0632
AFDye 647 Azide	Click Chemistry Tools	Cat# 1299
Click-&-Go Cell Reaction Buffer Kit	Click Chemistry Tools	Cat# 1263
Absolute ethanol	Fisher Scientific	Cat# BP2818100
Methanol (Optima LC/MS Grade)	Fisher Scientific	Cat# A456-500
Water (Optima LC/MS Grade)	Fisher Scientific	Cat# W7-4
Acetonitrile (Optima LC/MS Grade)	Fisher Scientific	Cat# A996-1
Formic Acid, 99.0+%, Optima LC/MS Grade	Fisher Scientific	Cat# A117-50
1.0 mm Zirconium Beads, Pre-Filled Tubes	OPS Diagnostics	N/A
Tissue-Tek O.C.T. Compound	VWR	Cat# 25608-930
Tissue-Tek Cryomold	VWR	Cat# 25608-916
RIPA buffer	Thermo Fisher Scientific	Cat# 89900
DC protein assay	Bio-Rad	Cat# 5000112
High-Capacity cDNA Reverse Transcription Kit	Thermo Fisher Scientific	Cat# 4368814
Power SYBR Green Master Mix	Thermo Fisher Scientific	Cat# 4368706
Nickel NTA Agarose Beads	Gold Biotechnology	Cat# H-350-5

(Continued on next page)

Continued

REAGENT or RESOURCE	SOURCE	IDENTIFIER
ProBlock Gold Bacterial 2D Protease Inhibitor Cocktail	Gold Biotechnology	Cat# GB-376-1
IPTG	Gold Biotechnology	Cat# I2481C5
Imidazole	Sigma-Aldrich	Cat# 56749
Glycerol	Sigma-Aldrich	Cat# G5516
Adenosine 5′-triphosphate disodium salt hydrate	Sigma-Aldrich	Cat# A2383-5G
Pyridoxal 5′-phosphate hydrate	Sigma-Aldrich	Cat# P9255
Triton X-100	Alfa Aesar	Cat# A16046-AE
L-SERINE (13C3, 99%; 15N, 99%)	Cambridge Isotopes	Cat# CNLM-474-H-0.1
L-THREONINE (13C4, 97-99%)	Cambridge Isotopes	Cat# CLM-2261-0.1
L-ASPARTIC ACID (13C4, 99%; 15N, 99%)	Cambridge Isotopes	Cat# CNLM-544-H-0.25
GLYCINE (13C2, 99%; 15N, 99%)	Cambridge Isotopes	Cat# CNLM-1673-H-0.25
L-CYSTEINE (13C3, 99%; 15N, 99%)	Cambridge Isotopes	Cat# CNLM-3871-H-0.1
L-METHIONINE (13C5, 99%)	Cambridge Isotopes	Cat# CLM-893-H-0.05
Eagle's Minimum Essential Medium (EMEM)	ATCC	Cat# 302003
Glucose-free DMEM	Thermo Fisher Scientific	Cat# A1443001
Trypsin	Sigma-Aldrich	Cat# T8003
GlutaMAX	Sigma-Aldrich	Cat# 35050061
Sucrose	VWR	Cat# 470302-808
QuantSeq 3' mRNA-seq Library Prep Kit	Lexogen	https://www.lexogen.com/store/quantseq-3-mrna-seq-library-prep-kits-for-illumina/
Fatty Acid Free BSA	Sigma-Aldrich	Cat# A8806
Seahorse XF Base Medium	Agilent Technologies	Part# 103335-100
Oligomycin	Sigma-Aldrich	Cat# 75351
Carbonyl cyanide 4-(trifluoromethoxy) phenylhydrazone (FCCP)	Sigma-Aldrich	Cat# C2920
Rotenone	Sigma-Aldrich	Cat# R8875
Antimycin A	Sigma-Aldrich	Cat# A8674
Acyl-coenzyme A synthetase from Pseudomonas sp.	Sigma Aldrich	Cat# A3352
Acyl-CoA synthetase, recombinant	Creative Enzymes	Cat# NATE-1682
BT0870_His6 (SPT)	This paper	N/A
Deposited data		
Metabolomic analysis	This manuscript	GNPS: MSV000087619
Raw HepG2 RNA sequencing data	This manuscript	Sequence Read Archive; SRA data: PRJNA808399
Raw Mouse Liver RNA sequencing data	This manuscript	Sequence Read Archive; SRA data: PRJNA808399
Experimental models		
Swiss Webster Mice	Taconic Biosciences	SW-F EF
Experimental models: Cell lines		
Human hepatocellular carcinoma cells (HepG2)	ATCC	HB-8065
Oligonucleotides		
qPCR: Mouse 18S rRNA forward	Thermo Fisher Scientific	GTAACCCGTTGAACCCCATT
qPCR: Mouse 18S rRNA reverse	Thermo Fisher Scientific	CCATCCAATCGGTAGTAGCG
qPCR: Mouse *CPT1a* (liver) *forward*	Thermo Fisher Scientific	CGTGACGTTGGACGAATC
qPCR: Mouse *CPT1a* (liver) *reverse*	Thermo Fisher Scientific	TCTGCGTTTATGCCTATC
qPCR: Mouse *CPT1b* (colon) *forward*	Thermo Fisher Scientific	GCACACCAGGCAGTAGCTTT

Continued

REAGENT or RESOURCE	SOURCE	IDENTIFIER
qPCR: Mouse *CPT1b* (colon) *reverse*	Thermo Fisher Scientific	CAGGAGTTGATTCCAGACAGGTA
pET21_BT0870_fwd	This paper	aattttgtttaactttaagaaggagatatacat ATGGGATTATTACAAGAGAAGTTAGCT
pET21_BT0870_rev	This paper	ggatctcagtggtggtggtggtggtgctcgag CAAAAGGTCTAAAGCTTTGAAAGCTTTC
Recombinant DNA		
Plasmid: pET21-BT0870	This paper	N/A
Software and algorithms		
Metaboseek (Helf et. al. 2022)	https://github.com/mjhelf/Metaboseek	Software version 0.9.6
GraphPad Prism	https://www.graphpad.com/scientific-software/prism/	
R software	https://cran.r-project.org/	R version 3.5.1
FastQC	https://www.bioinformatics.babraham.ac.uk/projects/fastqc/	Software version 0.11.5
Trimoomatic	(Bolger et al., 2014)	
DESeq2 package	(Love et al., 2014)	
GSEA	Broad Institute http://software.broadinstitute.org/gsea/index.jsp	
Salmon	(Patro et al., 2017)	Software version 0.7.2
pheatmap package	https://rdrr.io/cran/pheatmap/	
ImageJ, Fiji	(Schneider et al., 2012)	https://imagej.nih.gov/ij/
LAS X LS software Leica Application Suite (LAS)	https://www.leica-microsystems.com/products/microscope-software/p/leica-las-x-ls/	
BioRender	BioRender (2020)	https://www.biorender.com

RESOURCE AVAILABILITY

Lead contact
Further information and requests for resources should be directed to and will be fulfilled by the lead contact, Elizabeth Johnson (elj54@cornell.edu).

Materials availability
Plasmids and strains generated by this study are available through request to the lead contact, Elizabeth Johnson (elj54@cornell.edu) with a completed Material Transfer Agreement.

Data and code availability
- RNA-seq data have been deposited at the Sequence Read Archive under accession number SRA: PRJNA808399. Processed RNA-seq data are accessible in Tables S1C and S1F. Mass spectrometry data have been deposited at the Global Natural Product Social Molecular Networking (GNPS) database and are available under GNPS: MSV000087619. Accension numbers are listed in the key resources table.
- This paper does not report original code.
- Any additional information required to reanalyze the data reported in this paper is available from the lead contact upon request.

EXPERIMENTAL MODEL AND SUBJECT DETAILS

Bacterial strains and conditions
Bacteroides thetaiotaomicron strain VPI 5482 (wild type, BTWT) and the corresponding mutant strains (SLMUT) were prepared as described in (Goodman et al., 2009; Johnson et al., 2020). In brief, SLMUT consists of BTWT with a transposon inserted in a position 88% from the start of the gene BT0870, which is homologous to a gene with serine palmitoyl transferase (SPT) activity in *Bacteroides fragilis* (Wieland Brown et al., 2013) and the commonly-known SPT in yeast, resulting in inhibition of the canonical sphingolipid synthesis pathway in SLMUT.

BTWT and SLMUT were cultured in either brain heart infusion medium (BHIS) or minimal medium (MM) consisting of 13.6 g KH_2PO_4, 0.875g NaCl, 1.125 g $(NH_4)2SO_4$, 5 g glucose, (pH to 7.2 with concentrated NaOH), 1 mL hemin solution (500 mg dissolved in 10 mL of 1M NaOH, then diluted to final volume of 500 mL with water), 1 mL $MgCl_2$ (0.1M in water), 1 mL $FeSO_4 \cdot 7H_2O$ (1 mg per 10 mL of water), 1 mL vitamin K3 (1 mg/mL in absolute ethanol), 1 mL $CaCl_2$ (0.8% w/v), 250 μL vitamin B12 solution (0.02 mg/mL), and 5g L-cysteine hydrochloride anhydrous. Both media were prepared freshly and pre-reduced in the anaerobic chamber (70% N_2, 25% CO_2, and 5% H_2). Isotopic amino acid feeding studies were performed with the addition of 5 mM amino acid. For isotopic studies with labeled L-cysteine (13C3, 99%; 15N, 99%), the unlabeled L-cysteine was replaced with sodium thioglycolate.

To prepare the inoculation stock, 50 mL pre-warmed (37°C) BHIS was inoculated with either BTWT or SLMUT and cultured at 37°C under anaerobic conditions.

Laboratory animals

All procedures were carried out in accordance with protocols approved by the Cornell University Institutional Animal Care and Use Committee. For evaluating effects of bacterial-derived sphingolipids, 32 conventionally-raised, excluded flora, female 5-week-old Swiss Webster mice were purchased from Taconic Biosciences and allowed to habituate to the vivarium for 3 days after delivery. After acclimation, mice were weighed and randomly allocated to 4 treatment groups with 4 mice per cage and 2 cages per treatment. Mice were raised in autoclaved microisolator cages and housed in humidity and temperature-controlled rooms on a 12-hour light-dark cycle. In addition to the autoclaved sterile drinking water, 2 cages of mice (Chow group) were fed a breeder chow diet (5021 LabDiet) containing 23.7%-kcal fat, 53.2% carbohydrate, 23.1% protein; the other 6 cages of mice (PBS, BTWT[PAA] and SLMUT[PAA]) received a fat-free diet (Envigo, TD. 03314) containing 0%-kcal fat, 75.9% carbohydrate, and 24.1% protein for 4 weeks before oral administration of *B. thetaiotaomicron* strains. On the fifth week, all mice were kept on the same diet with oral administration of the *B. thetaiotaomicron* strains, as described below.

Food consumption and body weight were monitored weekly in a cage-wise and an individual manner, respectively. Autoclaved bedding and irradiated diet were replaced and supplied on a weekly basis.

HepG2 cell culture

Human hepatocellular carcinoma cells (HepG2) were maintained in EMEM supplemented with 10% (v/v) fetal bovine serum (FBS) and incubated in a humidified incubator with 5% CO_2 at 37°C unless otherwise indicated.

METHOD DETAILS

Preparation of bacteria for mouse gavage

In order to encourage bacterial consumption and metabolism of palmitic acid alkyne (PAA) to produce a suite of sphingolipids, 1 mL of BTWT and SLMUT inoculation stock was inoculated into 50 mL pre-warmed (37°C) MM supplemented with 25 μM PAA (BTWT[PAA] and SLMUT[PAA]). Cultures were grown overnight at 37°C. After a 24-h incubation, bacterial pellets were harvested by centrifugation at 4,000 x g for 20 minutes at room temperature, and the cells were pelleted and washed twice with sterile-filtered 1X phosphate-buffered saline (PBS) to remove residual PAA that was not taken up by the bacteria. The gavage concentration of both BTWT[PAA] and SLMUT[PAA] were adjusted to ~10^8 CFU per 200 μL of PBS.

For heat-killed BTWT[PAA] experiments, bacterial suspensions of BTWT[PAA] were diluted to approximate 10^8 CFU per 200 μL with PBS and autoclaved at 121°C for 15 minutes to kill the bacteria. Aliquots were cultured on Brain Heart Infusion agar plates supplemented with 10% defibrinated sheep blood to assess viability. Gram stains were done to assure the presence of bacterial cells in the autoclaved suspensions.

Oral gavage of BTWT[PAA] and SLMUT[PAA] to mice

After 4 weeks of dietary conditioning, mice in the BTWT[PAA] and SLMUT[PAA] groups were inoculated via daily oral gavage with the above prepared BTWT[PAA] and SLMUT[PAA] (200 uL per mouse) strains for 7 consecutive days to introduce labeled *B.thetaiotaomicron* lipids to the microbiomes of treated mice. Mice in the PBS group were gavaged with PBS for 7 days and served as the vehicle control group. On the day of sacrifice, mice in the PBS, BTWT[PAA], and SLMUT[PAA] groups were gavaged one last time with the corresponding treatments and then fasted for 5 h. Mice were culled by decapitation and colons were cut into 3 equal sections. Two pieces were stored in 2 mL screw-top tubes pre-filled with 1-mm zirconia beads (OPS diagnostics) and snap-frozen in liquid nitrogen, and the third piece of the colon was embedded in O.C.T compound (Sakura Finetek, Tokyo, Japan) and placed on ice. Similarly, 3 lobes of liver tissue were carefully cut and stored in the same manner as the colon. After stabilization on ice for one hour, the colon and liver portions embedded in O.C.T compound were rapidly frozen in 2-methylbutane chilled with liquid nitrogen. These frozen tissue blocks were wrapped in labeled foil and stored at -80°C until use.

Cu(I)-catalyzed azide-alkyne cycloaddition staining

One day before cryosectioning, the frozen tissue blocks were moved to the -20°C freezer to prevent damage during sectioning. A Leica CM3050S cryostat (Leica Microsystems K.K., Tokyo, Japan) was set to -25°C to maintain the optimal environment for the tissue block. After mounting the tissue blocks on the microtome, unfixed tissues were cryosectioned at 10 μm thickness and collected on Superfrost Plus microslides (VWR), followed by fixation in 4% paraformaldehyde in PBS at room temperature for

10 minutes. Slides were gently washed with 1% bovine serum albumin (BSA) in PBS, then subjected to permeabilization with isotonic Triton buffer (0.5% Triton X-100 in PBS) at room temperature for 10 minutes.

The click reaction was performed by incubating the slides in freshly-prepared click-reaction cocktail, prepared according to the manufacturer's instructions using the Click-iT Cell Reaction Buffer Kit (Click Chemical Tools) combined with Alexa Fluor-647 azide (Alexa Fluor 647 Azide, Triethylammonium Salt, Invitrogen) at the final concentration of 5 μM for 30 minutes at room temperature. To locate the tissue, cell nuclei were counterstained with 1 μg/mL Hoechst 33342 (Invitrogen), and coverslips were mounted onto slides using ProLong Gold antifade mountant (Thermo Fisher Scientific). Fluorescent images were acquired by using two color filter cubes: UV (359 nm/461 nm) for Hoechst 33342 and Cy5 (650 nm/670 nm) for AF647 on a Leica DM500 fluorescence microscope (Leica, Buffalo Grove, IL) or a Zeiss LSM 880 (Carl Zeiss, Jena, Germany) inverted confocal microscope. All images were analyzed using Fiji Image J software (Schindelin et al., 2012).

Tissue lipid extraction for LC-HRMS analysis

Mouse livers and colons were homogenized with PBS in tubes with sterile 1 mm zirconium beads (OPS diagnostics) using a bead beater homogenizer (BioSpec products) for 3 minutes, the intestinal samples were homogenized for one more round to ensure homogeneity. The tissues were placed on ice right after the homogenization, and 10 μL of the homogenate was added with 90 μL RIPA buffer (Thermo Scientific) for protein concentration determination using the Lowry protein assay (BioRad). We then transferred 5,000 μg of protein per liver and 1,000 μg of protein per colon to fresh 1.5 mL tubes. Tissue lysates were frozen in liquid nitrogen and lyophilized to dryness. Next, 1 mL of pure HPLC-grade methanol (Fisher Scientific) was added to the sample, which was then subjected to ultrasonic assisted extraction for 5 minutes on/off cycles of 3 seconds on and 2 seconds off, at 100% power on a Qsonica ultrasonic processor. The obtained mixture was then subjected to overnight extraction in methanol on an end-over-end rotor. Samples were then spun at 18,000 x g for 30 minutes at 4°C, 950 μL supernatant was transferred to a new 1.5 mL tube. The collected supernatant was evaporated to dryness with a SpeedVac vacuum concentrator (Thermo Fisher Scientific) and reconstituted in 200 μL of pure HPLC-grade methanol (Fisher Scientific). The obtained extracts were then centrifuged for 30 min at 18,000 x g at 4°C, 150 μL of the concentrated supernatant was transferred to HPLC vial with an insert (Thermo Fisher Scientific) and stored at -20°C until HPLC-HRMS analysis.

Mass spectrometry analysis

High-resolution LC−MS analysis was performed on a Thermo Fisher Scientific Vanquish Horizon UHPLC System coupled with a Thermo Q Exactive HF hybrid quadrupole-orbitrap high-resolution mass spectrometer equipped with a HESI ion source. 3 μL of extract was injected and separated using a water-acetonitrile gradient on a Kinetex EVO C18 column (150 mm × 2.1 mm, particle size 1.7 μm, part number: 00F-4726-AN) maintained at 40°C. Solvent A: 0.1% formic acid in water; Solvent B: 0.1% formic acid in acetonitrile. A/B gradient started at 10% B for 3 min after injection and increased linearly to 100% B at 17 min and held at 100% B for 10 min, using a flow rate 0.5 mL/min. Mass spectrometer parameters: spray voltage 3.5 kV for positive mode and 3.0 kV for negative mode, capillary temperature 380°C, prober heater temperature 400°C; sheath, auxiliary, and spare gas 60, 20, and 1, respectively; S-lens RF level 50, resolution 240,000 at m/z 200, AGC target 3×10^6. Tandem mass spectrum analysis was carried out with an inclusion list of differential features on PRM mode utilizing the same parameters (vide supra) with the following additions or adjustments: AGC target 2×10^5, max ion injection time: 500 ms, isolation window: 0.7 m/z, collision energy: 35 NCE. The instrument was calibrated with positive and negative ion calibration solutions (Thermo- Fisher). Each sample was analyzed in positive and negative modes with m/z ranging from 100 to 1,200.

Untargeted metabolomic analysis

RAW files generated from HPLC-HRMS acquisitions were converted to mzXML files utilizing MSconvertGUI software (proteowizard.sourceforge.net). Differential metabolic features were determined by subjecting mzXML files to Metaboseek Software version 0.9.6 (metaboseek.com) (Helf et al., 2022) utilizing the XCMS package with all values set to default parameters which are as follows: Peak Detection: ppm 4, peakwidth 320, snthresh 3, prefilter 3100, fitgauss FALSE, integrate 1, firstBaselineCheck TRUE, noise 0, mzCenterFun wMean, mzdiff -0.005, workers 4. Peak filling: METABOSEEK, ppm_m 5, rtw 5, rtrange TRUE, areaMode FALSE. Feature Grouping: minfrac 0.2, bw 2, mzwid 0.002, max 500, minsamp 1, usegroups FALSE. CAMERA and RT correction were not used. Differential molecular features were sorted using the minFoldOverCtrl, minInt, and Fast_Peak_Quality filters. Differential features were subjected to manual curation to remove adducts, isotopes, and false positives. The curated list of molecular features were assigned molecular formulas and then subjected to tandem mass spectrometry for further elucidation. LC-MS files have been deposited to the GNPS Web site (massive.ucsd.edu) with MassIVE ID numbers MSV000087619. Data are also available in Table S1G (liver) and Table S1H (colon).

Liver histology

Dissected liver samples from each mouse were fixed in 4% paraformaldehyde, embedded in paraffin, sectioned at 5 μm, and stained with hematoxylin and eosin (H&E) after deparaffinization. H&E-stained sections were imaged under Leica DM500 fluorescence microscope (Leica, Buffalo Grove, IL) at 20X magnification.

CellPress
OPEN ACCESS

qPCR

Total RNA was isolated using Trizol (Invitrogen, Carlsbad, CA) after tissue homogenization in PBS, followed by the cDNA synthesis using the High Capacity cDNA Reverse Transcription Kit (Applied Biosystems, Foster City, CA). Relative mRNA expression was determined using the ViiA 7 real-time PCR system (Life Technologies Corporation) with Power SYBR Green PCR Master Mix (Applied Biosystems, CA, US) as follows: one cycle at 95°C (10 minutes), 40 cycles of 95°C (15 seconds) and 58°C (1 minute). Relative mRNA expression levels were normalized to that of 18S rRNA (internal control) on the basis of the cycle threshold (Ct) value.

Recombinant *Bt*SPT-His6 purification

BT_0870 (*Bt*SPT) was PCR-amplified with primers pET21_BT0870_fwd and pET21_BT0870_rev, listed in the key resources table, and the PCR product underwent restriction digestion followed by ligation into the pET21a (MilliporeSigma, Massachusetts, USA) vector via *Xho*I and *Nde*I restriction sites. Successful integration was verified by sequencing and the plasmid was transformed into BL21 *E. coli*, Colonies were selected in Lennox Broth (LB)-agar plates containing 100 μg/mL carbenicillin (Carb). Two separate colonies were picked into 2 x 5 mL LB+Carb in a 14-mL culture tube and incubated at 37°C at 250 rpm for 16 hours. The 10-mL culture was added to 1 L Terrific Broth (TB)+Carb with 4% glycerol in a 2-L flask and incubated at 37°C at 250 rpm until OD 1.0. The temperature was then reduced to 20°C and IPTG (GoldBio) was added to a final concentration of 100 μM. Shaking continued for an additional 18 hours. Cells were harvested with centrifugation at 5,000 x g at 4°C for 10 minutes, and resuspended in 80 mL of lysis buffer (20 mM potassium phosphate pH 7.2, 125 mM sodium chloride, 10 mM imidazole, 25 μM pyridoxal phosphate, and 1X ProBlock Gold Bacterial 2D Protease Inhibitor Cocktail (GoldBio)). Cells were sonicated with a probe sonicator on an ice bath for 4 minutes (total on time), cycling between 2 seconds on and 2 seconds off. The lysed cells were centrifuged at 20,000 x g for 20 minutes at 4°C. The soluble fraction was applied to 2 mL Ni-NTA (GoldBio) for 20 minutes on an end-over-end rotator. The slurry was moved to a column and drained via gravity. The Ni-NTA was washed with 25 mL lysis buffer without protease inhibitor and then bound protein was eluted with 15 mL elution buffer (20 mM potassium phosphate pH 7.2, 125 mM sodium chloride, 200 mM imidazole, 25 μM pyridoxal phosphate, 10% (v/v) glycerol). Eluent was concentrated to approximately 50 mg/mL with an Amicon Ultra-15 30K MW cutoff spin filter, aliquoted and flash-frozen with liquid nitrogen, and stored at -80°C until further use. Purity was verified with SDS-PAGE via Coomassie staining.

Synthesis of 3-ketosphinganine derivatives

Assay conditions for the synthesis of 3-ketosphinganine derivatives (3-KS) were 50 mM potassium phosphate pH 7.5, 10 mM adenosine triphosphate, 2 mM coenzyme A, 5 mM magnesium chloride, 0.05% (v/v) Tween 20, 250 μM palmitic acid alkyne (Click Chemistry Tools), and 0.025 U of acyl-coenzyme A synthetase from Pseudomonas sp. (Sigma Aldrich) to a final volume of 1 mL and incubated at 37°C for 2 hours. A final concentration of 2 mM of an amino acid was added along with 1 μL of *Bt*SPT-His6 solution and incubated for 3 additional hours at 35°C. Aliquots of 10 μL of each 1 mL reaction were prepared for mass spectrometry analysis.

Conversion of 3-KS derivatives to complex SLs

BT-SLMUT was inoculated into 20 mL BHIS media and incubated at 37°C in an anaerobic bottle for 16 hours to produce a starter culture. We then added 1 mL of the starter culture to minimal culture media (100 mM potassium phosphate pH 7.2, 15 mM sodium chloride, 8.5 mM ammonium sulfate, 200 μM magnesium chloride, 1.5 μM ferrous sulfate, 75 μM calcium chloride, 500 ug/mL L-cysteine, 20 μg/mL vitamin B12, 1 μg/mL menadione, 1 μg/mL hemin, 0.5 μg/mL resazurin, 1% (w/v) glucose) and incubated the culture at 37°C in an anaerobic bottle for 20 hours. Products for the 3-KS derivative enzymatic reactions were added directly to the BT-SLMUT cultures via needle through rubber septa, and incubation at 37°C was continued for an additional 24 hours. All of the following steps occurred aerobically. Cultures were transferred to 50-mL centrifuge tubes and centrifuged at 4,000 x g for 5 minutes at 20°C. The spent culture medium was carefully removed, and the bacterial pellet was resuspended in 1 mL PBS and transferred to 1.5 mL centrifuge tubes. Bacteria was collected again at 4,000 x g for 5 minutes at 20°C and the supernatant removed. Samples were immediately frozen in liquid nitrogen and underwent metabolite extraction.

Enrichment of homoserine dihydroceramide

Ketosphingoid bases were prepared (*vida supra*) and supplied to SLMUT (or uninduced BTiSPTΔ1526) at 3L scale and cultured (*vida supra*) for 24 hours. Bacteria were collected via centrifugation and methanol-extracted overnight. The methanolic extract was dried and resuspended in 2 mL water, and the sphingolipid was extracted via biphasic extraction with 120 mL ethyl acetate. The organic phase was dried and resuspended with 2 mL of silica gel mobile phase, 95:4:1 ethyl acetate:methanol:acetic acid. The extract was loaded onto 11 g of silica gel (Sigma Aldrich, Cat# 60741-1KG) loaded on a gravity column (Sigma Aldrich, Cat# Z163961) preequilibrated with silica gel mobile phase. We then collected and dried 25-mL fractions. The dried fractions were resuspended in methanol and analyzed via LC-MS. Fractions containing the target sphingolipid were pooled, dried, and resuspended in 200 μL of methanol. The crudely isolated target sphingolipid was further purified with a ZORBAX Eclipse XDB C18 Semi-prep column (Agilent, Cat# 990967-202) using a water-methanol (A-B) gradient: 0-2 minutes 50% B, 2-25 minutes increase linearly to 100% B, 25-49 minutes hold 100% B, maintaining the column at 50°C with a Thermo Fisher Scientific Vanquish UHPLC equipped with a Fraction Collector (Cat# VF-F11-A-01). Fractions containing the target sphingolipid, as monitored in real-time via a TSQ Quantis Triple Quadrupole Mass Spectrometer, were pooled, dried, and resuspended in 200 μL absolute ethanol (Fisher Chemicals, Cat# BP2818) and stored at -20°C until further use. Area under the curve measurements from ion traces were used to approximate the concentration of the lipid

against a C16 Dihydroceramide (d18:0/16:0) synthetic standard (Avanti Lipids, Birmingham, AL). The purity of the fraction was estimated at 84% and the detected masses unique to the sample are listed in Table S1I.

In vitro treatment of homoserine dihydroceramide

HepG2 cells were plated into 6-well culture plates at 5×10^4 cells per well for 24 h. After adhesion, the medium was replaced by serum-free medium containing 0.25% lipid-free bovine serum albumin (BSA). Subsequently, cells were treated with an oleate/palmitate mixture (2:1 molar ratio, 0.75 mM as the final concentration) in combination with 10 mM sucrose in glucose-free DMEM supplemented with 2 mM GlutaMAX and 1 mM sodium pyruvate for 48 h. Cells were then treated with either ethanol (vehicle) or 50 μM fractionated homoserine dihydroceramide (*vida supra*) for 24 h in glucose-free DMEM supplemented with 2 mM GlutaMAX and 1 g/L glucose as EMEM.

RNA sequencing and analysis

Total RNA was extracted from the mouse liver tissue and HepG2 cells using the TRIzol reagent (Invitrogen, Carlsbad, CA) in conjunction with the RNA Clean & Concentrator Kit (Zymo Research) following the manufacturer's instructions. The optional on-column Dnase treatment from the kit was carried out to remove the trace amount of genomic DNA during RNA extractions. After qualification and quantification, libraries were prepared using the QuantSeq 3' mRNA-Seq Library Prep kit FWD for Illumina (Lexogen, Vienna, Austria) according to the manufacturer's instructions. Samples were subjected to 75 bp single-end sequencing using the Illumina NextSeq 500 platform. Quality of raw read data was checked using FastQC (version 0.11.30). Reads were then aligned to the human (hg129) or mouse (mm9) genome using the STAR aligner (Dobin et al., 2013) and transcript abundance was estimated using Salmon (Patro et al., 2017). For the mouse samples, the average read coverage was 26,040,945 million reads/sample with an average of 75% of the reads successfully mapping to the mouse genome. For the human HepG2 cell line samples, the average read coverage was 20,1443,143 reads/sample with an average of 76% of the reads successfully mapping to the human genome. Sequenced reads were normalized to RPKM, and differentially expressed genes between BTWT[PAA] and SLMUT[PAA] mouse hepatic tissue or between vehicle control (EtOH) and hsDHCer treated HepG2 cells were determined using DESeq2 (Love et al., 2014). Significantly differentially expressed genes were determined using a Benjamini-Hochberg adjusted p-value cutoff of $p < 0.05$ and pathway enrichment was determined by using these genes as an input into Gene Set Enrichment Analysis (GSEA) (Subramanian et al., 2005). GSEA was performed using GSEA (version 2.0.14) software with 1000 gene-set permutations using the gene-ranking metric t-test with the collections H.all.V5.2.symbols (Hallmarks) or c5.all.v6.1.symbols (C5, GO term) signatures. Enrichment sets with a false discovery rate (FDR) <0.05 were considered significant. The normalized enrichment score (NES) was the primary metric from GSEA for evaluating differentially expressed pathways. Heatmaps were generated from z-score normalized RPKM values or $\log_2$ fold change expression and output using heatmap R package on selected sets of genes.

Seahorse extracellular flux measurement

HepG2 cells were seeded in an XF 96 well plate at 2×10^4 cells/well for 24 h, followed by the treatment as described above. On the day of the assay, cells were washed one time with PBS and media was replaced with 165 μL Seahorse XF base medium (Agilent 102353-100) containing 1 g/L glucose, 1 mM sodium pyruvate and 0.1% BSA. After incubating in a non-CO_2 incubator at 37°C for 1 hour, the cell plate was inserted into a Seahorse XF 96 Analyzer (Agilent Technologies, Santa Clara, CA). After 3 basal measurements, oligomycin was injected for a final concentration of 1 μM to inhibit ATP synthesis. Next, FCCP was injected with a final concentration of 1 μM to determine maximal respiratory capacity. Finally, a mixture of rotenone and antimycin was injected to inhibit all mitochondrial respiration (final concentration of 0.5 μM each). Protein concentration of the cells was measured after the analysis and used to normalize the oxygen consumption rate (OCR).

QUANTIFICATION AND STATISTICAL ANALYSIS

Statistical analyses were carried out using R-Studio or GraphPad Prism version 9.0. When comparing two groups, significance was determined using a two-tailed Student's *t* test. Significance tests for comparing more than one experimental group were determined using a one-way analysis of variance (ANOVA) with Tukey tests used for post hoc analysis. For RNA-seq analysis, differential expressed genes (DEGs) between experimental conditions in either HepG2 cells or liver tissue were determined using DESeq2 (Love et al., 2014) and significance was determined by setting a false discovery rate (FDR) < 0.05 using the Hochberg-Benjamini procedure. DEGs in HepG2 cells and hepatic tissue were used as input into gene set enrichment analysis and enriched gene sets with an absolute normalized enrichment score (NES) $\geq$ 1 and FDR < 0.05 were highlighted. Results are presented as mean ± SD, unless otherwise indicated. Statistical significance was assigned as ***$p \leq 0.001$; **$p \leq 0.01$; *$p \leq 0.05$; $p > 0.05$: ns (not significant).